A neuronal network model of primary visual cortex explains spatial frequency selectivity

Wei Zhu · Michael Shelley · Robert Shapley

Abstract We address how spatial frequency selectivity arises in Macaque primary visual cortex (V1) by simulating V1 with a large-scale network model consisting of $O(10^4)$ excitatory and inhibitory integrate-and-fire neurons with realistic synaptic conductances. The new model introduces variability of the widths of subregions in V1 neuron receptive fields. As a consequence different model V1 neurons prefer different spatial frequencies. The model cortex has distributions of spatial frequency selectivity and of preference that resemble experimental findings from the real V1. Two main sources of spatial frequency selectivity in the model are the spatial arrangement of feedforward excitation, and cortical nonlinear suppression, a result of cortical inhibition.

Keywords Spatial frequency selectivity ·
Large-scale neuronal network · Feedforward input ·
Cortical excitation · Cortical inhibition ·
Simple/complex cells

W. Zhu (✉) · M. Shelley
Courant Institute of Mathematical Sciences,
New York University, 251 Mercer Street,
New York, NY 10012, USA
e-mail: wzhu@cims.nyu.edu

M. Shelley
e-mail: shelley@cims.nyu.edu

R. Shapley
Center for Neural Science, New York University,
4 Washington Place, New York, NY 10003, USA
e-mail: shapley@cns.nyu.edu

1 Introduction

Spatial frequency selectivity is an important property of neurons in primary visual cortex, V1 (DeValois and DeValois 1988; von der Heydt et al. 1992). Retinal ganglion cells are broadly tuned for spatial frequency because of the center-surround organization of their receptive fields (Kuffler 1953; Enroth-Cugell and Robson 1966; Rodieck 1965). However, the spatial frequency tuning of V1 neurons is often much narrower than that of retinal ganglion cells (Campbell et al. 1969; Movshon et al. 1978; DeValois et al. 1982). In this paper we offer a theoretical explanation for cortical spatial frequency selectivity based on computer simulations with a large-scale network model of the visual cortex. Similar cortical network models can be found in (Troyer et al. 1998; Chance et al. 1999; McLaughlin et al. 2000; Tao et al. 2004, 2006).

The large-scale model we used has a realistic spatial pattern of synaptic connections, like previous large-scale models that our group developed (McLaughlin et al. 2000; Tao et al. 2004, 2006). This model also implements sparse connections between excitatory cortical neurons and all the other neurons following the data of Holmgren et al. (2003) and the theoretical approach of Tao et al. (2006). What makes the present model different is how V1 receptive fields are constructed in this model. In previous models, all V1 neurons had receptive field sub-regions with the same width (Troyer et al. 1998; McLaughlin et al. 2000; Tao et al. 2004). However, in the present model, receptive field sub-regions vary in width over a four-fold range. As a consequence, different neurons have different spatial frequency preferences, as in V1. The patterns of Lateral Geniculate Nucleus (LGN) inputs to the different V1

receptive fields do not explain fully the selectivity for spatial frequency observed in V1 cortex, as we demonstrate in Results. Cortical interactions are needed to explain spatial frequency selectivity. The new model presented here emulates many properties of V1: the distribution of spatial frequency selectivity and preference, as well as the relative numbers of simple and complex cells, the range and distribution of firing rates, and also the properties of orientation selectivity.

The classical picture explained cortical spatial selectivities as consequences of additive convergence of LGN input onto V1 cells, consistent with the hypothesis that V1 cells are linear spatial filters of narrow bandwidth (Robson 1975; DeValois and DeValois 1988; DeAngelis et al. 1995; Dayan and Abbott 2001). But here we offer a different explanation: cortical suppression of non-preferred responses. This idea was proposed originally based on experimental results (cf. Bredfeldt and Ringach 2002; Ringach et al. 2002b). Cortical selectivity in the model comes about because of nonlinear suppression caused by cortico-cortical inhibition (see also Lauritzen and Miller 2003). The good agreement between the responses of the model and the real cortex to many different kinds of stimuli suggests that, in the real cortex, cortical inhibition may be important for spatial feature selectivity.

2 Methods

2.1 Large-scale model

Our model resembles the models described in (McLaughlin et al. 2000; Wielaard et al. 2001; Tao et al. 2004, 2006): a large-scale neuronal network of V1 layer 4cα, consisting of 16,384 integrate-and-fire neurons, 75% of which are excitatory and 25% of which are inhibitory. The membrane potential of each V1 neuron is governed by the following equation:

$$\frac{dv_\sigma^j}{dt} = -g_R \left(v_\sigma^j - V_R\right) - g_{\sigma E}^j(t) \left(v_\sigma^j - V_E\right) - g_{\sigma I}^j(t) \left(v_\sigma^j - V_I\right)$$
$$= -g_T^j(t) \left[v_\sigma^j - V_S^j(t)\right], \quad (1)$$

where $\sigma = E, I$ represent excitatory, inhibitory neurons respectively; v_E^j represents the membrane potential of an excitatory neuron at the location within the cortical layer indexed by j. When $v_\sigma^j > V_{Threshold}$, a spike is fired. Membrane capacitance is assumed here to be a fixed constant, and is absorbed into the conductances so that conductances have the units of rate, per second. In Eq. (1), $g_T = g_R + g_E + g_I$ is the total membrane conductance and $V_S = (V_E g_E + V_I g_I)/g_T$ is

the effective reversal potential. In the high conductance state of this model, a neuron's membrane potential tracks very closely the effective reversal potential (cf. Shelley et al. 2002).

Voltage is normalized so that $V_R = 0$ and $V_{Threshold} = 1$. Therefore, the reversal potentials of the synapses V_E and V_I are normalized to have the values $\frac{14}{3}$ and $-\frac{2}{3}$ respectively. The leakage conductance g_R is set to be $g_R = 50$, and the four cortico-cortical conductances satisfy the following relations:

$$g_{EE}^j(t) = g_{lgn}^j(t) + g_{noise}^j(t)$$
$$+ S_{EE}^j \sum_k a_{j-k} p_{j-k} \sum_m G_E\left(t - t_m^k\right),$$

$$g_{EI}^j(t) = S_{EI}^j \sum_k b_{j-k} \sum_m G_I\left(t - t_m^k\right),$$

$$g_{IE}^j(t) = g_{lgn}^j(t) + g_{noise}^j(t)$$
$$+ S_{IE}^j \sum_k a_{j-k} p_{j-k} \sum_m G_E\left(t - t_m^k\right),$$

$$g_{II}^j(t) = S_{II}^j \sum_k b_{j-k} \sum_m G_I\left(t - t_m^k\right). \quad (2)$$

The spatial coupling coefficients a_{j-k}, b_{j-k} are each Gaussian functions of cortical distance between cells j, k. The Gaussian length scales for excitation and inhibition are 200 and 100 μm, respectively, derived from neuroanatomical measurements as in McLaughlin et al. (2000).

In our network, we needed to introduce 50% sparsity for excitatory-excitatory and excitatory-inhibitory connections in order to obtain selectivities like those seen in V1. These sparse cortico-cortical connections are suggested by experimental data (Holmgren et al. 2003). However, following the experimental data of Holmgren et al and also Beierlein et al. (2003), the model's inhibitory-excitatory and inhibitory-inhibitory connections were not sparse at all. Specifically, each excitatory neuron is connected to approximately half of all the other neurons (excitatory or inhibitory) within its synaptic target zone and synaptic weights of the sparser connections are assigned double strength to maintain the same level of excitation as dense connections. To be precise, in Eq. (2) the conductance terms $g_{EE}^j(t)$ and $g_{IE}^j(t)$ contain a sparsity factor: $p_i = 0, 1$ that takes one of its two possible values randomly, with 0.5 probability. The sparsity factor introduces randomness and sparsity into the connections between excitatory neurons and all the other neurons.

Two issues about sparsity need to be specified. First, the 50% connectivity in our network is larger than what was used in Tao et al. (2006). The main reason is due to the introduction of width-variability, which could lead to effective sparsity in our present model. This argument will be detailed later. Second, based on our numerical implementation, the amount of sparsity is one of the crucial factors that affect the network of our model. Experiments with full connection (i.e., 0% sparsity) of our model demonstrate clearly the bi-stability phenomenon discussed in (Cai et al. 2004).

In the present model the values in the conductance coupling matrix in Eq. (2) are: recurrent excitation's coefficient $S_{EE} = 0.1$ for its minimum, and $S_{EE} = 45.0$ for its maximum value (for the cells that receive no LGN input); the coupling strength for inhibitory synapses onto excitatory neurons $S_{EI} = 80$; $S_{IE} = 0.1 - 46$ for the range between its minimum and maximum values; $S_{II} = 65$.

The visual stimuli we consider in this work are drifting gratings. Drifting gratings and contrast reversals are two frequently used stimuli to study orientation selectivity, spatial frequency selectivity as well as others. Many real data are obtained by using these stimuli. To compare with the data, we employ drifting gratings that read as follows, $I(x, t) = I_0[1 + \epsilon \sin(\overrightarrow{\xi} \cdot x - \omega t + \phi)]$. $\overrightarrow{\xi} = \xi(\cos\theta, \sin\theta)$ and $\xi = 2\pi k$ with k the spatial frequency of the grating in cycles/degree. $\theta \in [0, 2\pi)$ is the grating's orientation, $\phi \in [0, 2\pi)$ its spatial phase. $\omega = 2\pi f$ where f is the temporal frequency of the drift in cycles/second. In all computational experiments in this paper we used $f = 8 Hz$. I_0 is the mean luminance, and ϵ the contrast. The visual stimulus is projected onto the retina and the output of the retina, the retinal ganglion cells, excite cells in the LGN.

2.2 LGN synaptic drives

Each V1 neuron, excitatory or inhibitory, receives LGN input from a group of LGN cells. The number of LGN cells driving a model V1 neuron is drawn from a uniform distribution with the range [0, 30] (Tao et al. 2004, 2006). The present model also adopts the following assumption: those V1 neurons receiving the weakest LGN inputs are given the strongest cortico-cortical excitatory postsynaptic drive and external noise; cortical synaptic coupling strength is in a linear anti-proportion with that of the LGN inputs (Tao et al. 2004).

Optical imaging measurements show that in the superficial layers 2/3 of V1 there are pinwheel patterns of orientational preference on the cortex; neurons of like-orientation preference reside along the same radial

spoke of a pinwheel, with the preferred angle sweeping through 180° around the pinwheel. These pinwheels tile the cortical layer, separated from each other by approximately 500 μm. Because of the known columnar architecture of V1, we assume that there is a similar pinwheel structure in layer 4C (McLaughlin et al. 2000; Tao et al. 2004). We built a pinwheel structure into the model by tying the preferred orientation angle of the LGN input to a given 4C neuron to the neuron's location in the layer with respect to the pinwheel pattern. In the model, four pinwheels, chosen with alternating handedness, are placed upon a square, as in previous versions.

In our present model, the spatial pattern of LGN input to a single model neuron is side-by-side elongated sub-regions. We put spatial frequency information into the construction of those elongated regions by allowing different sub-region widths. There are optical imaging data (Sirovich and Uglesich 2004) and single unit data (DeAngelis et al. 1999) that indicate there is an apparently random distribution of spatial frequency preference with some local positive spatial correlation. To be consistent with these data, we also divide the network into many clusters of cells, inside each of which the V1 neurons share the same width of their LGN input arrays. Clusters of different width are arranged randomly across the V1 layer. Specifically, we assign 16×16 clusters for our network, one-sixth of which are with width one, one third with width two and the remaining width four. Here "width one" means that the elongated sub-region receives at most one LGN cell in the direction orthogonal to its long axis. Moreover, the spatial pattern of LGN inputs to each V1 neuron is set randomly to have even or odd symmetry, i.e, for an even symmetric neuron, the LGN input to the elongated sub-regions could be of the form ON-OFF-ON or OFF-ON-OFF. Such a random assignment of symmetry is also compatible with cortical data (DeAngelis et al. 1999; Ringach 2002). Some typical LGN input patterns in our model are illustrated in Fig. 1.

Given the group of LGN cells for a V1 neuron, the LGN conductance input to this V1 neuron is just the sum of the LGN cells' firing rates filtered through the LGN-V1 synapse. For instance, the LGN conductance received by the jth V1 neuron can be written as follows:

$$g_{lgn}^{j}(t) = c_E \sum_k \sum_l \mathbf{G}_E\left(t - s_l^k\right), \qquad (3)$$

where the first sum runs over all the LGN cells in the assigned group for the jth V1 neuron, and the second sum $\sum_l \mathbf{G}_E(t - s_l^k)$ characterizes the postsynaptic conductances induced by the kth LGN cell in that group,

Fig. 1 Four kinds of V1 neuron receptive fields in our model. In this figure, *red/green disks* represent ON/OFF LGN cells. The receptive field on the *top left* is an example of the type "width one", which results in strong LGN input for high spatial frequency stimulus. The remaining receptive fields correspond to width two and width four. The bottom two receptive fields also show even symmetry and odd symmetry

(61, 97)

(97, 59)

(33, 33)

(97, 41)
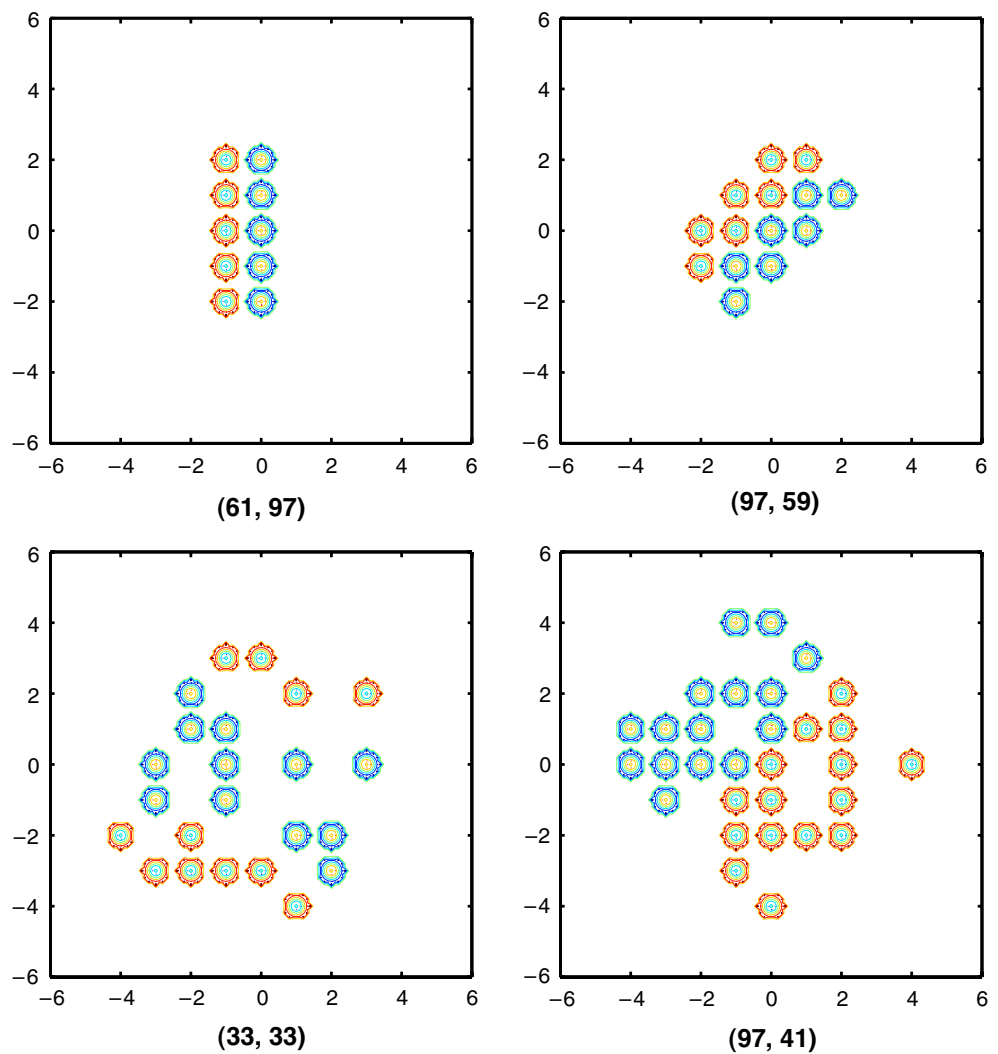
where the sequence s_l^k denotes the spike times of the kth LGN cell.

The spike times, s_l^k, are given by inhomogeneous Poisson processes whose rates $R_k(t)$ are characterized by linear, threshold, spatial-temporal filters of the visual stimulus $I(x, s)$ as follows:

$$R_k^{\pm}(t) = \left[R_B \pm \int_0^t ds \int_{\mathbf{R}^2} dx G(t-s) A(|x_k - x|) I(x, s) \right]^+,$$
(4)

where $R_k^+(t)/R_k^-(t)$ represent the rate of an ON/OFF LGN cell; $[...]^+$ represents rate rectification, i.e., $[x]^+ = x$ if $x > 0$ and $[x]^+ = 0$ if $x < 0$; and LGN background firing rate $R_B = 15$.

The LGN-cortex coupling coefficient c_E is set to a value of 0.12, chosen to fit the firing rates of simple cortical cells. The synaptic filter's impulse response

(or equivalently the unitary excitatory post-synaptic conductance, EPSC, time course) $\mathbf{G}_E$ is chosen to be

$$\mathbf{G}_E(t) = \frac{1}{6\tau_\sigma} \left(\frac{t}{\tau_\sigma} \right)^3 \exp\left(-\frac{t}{\tau_\sigma} \right) H(t),$$
(5)

where H is the Heaviside function with $H(x) = 1$ if $x > 0$, and $H(x) = 0$ if $x <= 0$.

The temporal kernel $G(t)$ and the spatial kernel $A(x)$ of an LGN cell are chosen to be consistent with experimental measurements with the following forms:

$$G(t) = \frac{t^5}{\tau_0^6} \left[\exp\left(-\frac{t}{\tau_0} \right) - \left(\frac{\tau_0}{\tau_1} \right)^6 \exp\left(-\frac{t}{\tau_1} \right) \right],$$
(6)

$$A(x) = \frac{a}{\pi \sigma_a^2} \exp\left(-\left| \frac{x}{\sigma_a} \right|^2 \right) - \frac{b}{\pi \sigma_b^2} \exp\left(-\left| \frac{x}{\sigma_b} \right|^2 \right),$$
(7)

with $\tau_0 = 3$ ms, $\tau_1 = 5$ ms, $\sigma_a = 0.066^0$, $\sigma_b = 0.093^0$, and $a = 1.0, b = 0.74$. The results of the cortical model simulations were not sensitive to the LGN spatial parameters. We increased σ_b by a factor of 2 and it had only a small quantitative effect on the cortical transformation of spatial frequency and orientation.

2.3 Cortico-cortical drives and external noise

The Egalitarian model (Tao et al. 2004) is a large-scale computational model developed by us and our colleagues to produce simple and complex cells (Hubel and Wiesel 1962; DeValois and DeValois 1988) in a single sheet of cortical neurons. It involved feedforward and recurrent excitatory and inhibitory connections that were egalitarian in the sense that there were no forbidden connections as there would be in hierarchical models. As in the Egalitarian model (Tao et al. 2004), we model each cortico-cortical excitatory postsynaptic conductance as a combination of 50% ($AMPA$) and 50% ($NMDA$). The use of slower NMDA-type excitation is to achieve cortical stability when there are strong recurrent excitatory connections. Each inhibitory postsynaptic conductance was modeled as the combination of 50% fast $\gamma-$ aminobutyric acid type A ($GABA_A$) and 50% of a slower ($GABA_A$) inhibition to simulate the results of Gibson et al. (1999).

The postsynaptic conductance change (PSC) functions for $AMPA$, and the $GABA_A$ faster and slower inhibition share the form of the Eq. (5) with different values of τ: 1, 1.67 and 7 ms, respectively, while the function for $NMDA$ reads (Koch 1999):

$$\mathbf{G}_{NMDA}(t) = \frac{1}{\tau_1 - \tau_2} \left[\exp\left(-\frac{t}{\tau_1} \right) - \exp\left(-\frac{t}{\tau_2} \right) \right] H(t),$$
(8)

where $\tau_1 = 80ms$, $\tau_2 = 2ms$.

The external noise is the sum of many spike time sequences which are generated by independent, homogeneous Poisson processes. For simplicity, we also model external noise by employing the same PSC functions as for the cortico-cortical postsynaptic drives. The external noise term is required and plausible from the following reasoning. When there is no visual input as when the eye views a blank screen, there is spontaneous

spike-firing activity in V1 cortex, for example see (Ringach et al. 2002a), among others. There is a higher level of spontaneous activity in complex cells than in simple cells. In the model, the needed excitatory drive for spontaneous activity in complex cells must come from external, presumed cortico-cortical, noise, as also in (Wielaard et al. 2001; Tao et al. 2004).

2.4 Global measures of spatial selectivity: low spatial frequency variance

To quantify spatial frequency selectivity we utilize the quantity called low spatial frequency variance (LSFV) introduced by Xing et al. (2004). LSFV is a global measure to assess the degree of low spatial frequency attenuation. It can capture the global shape of a spatial frequency tuning curve while standard bandwidth (the half-width at half-height of the tuning curve) only describes the shape near the peak (preferred) spatial frequency. The LSFV measure is smaller the more a cell is tuned for spatial frequency; LSFV has a value of 0 for the most tuned cells; for an untuned, low-pass neuron LSFV is equal to 1/3 (as shown in Xing et al. 2004 with examples of data).

The calculation of a V1 neuron's LSFV from its spatial frequency tuning curve proceeds in two steps. The first step is to fit the given spatial frequency tuning by the following Difference-of-Gaussians function

$$R(SF) = R_0 + K_e \exp\left(-\frac{(SF - \mu_e)^2}{2\sigma_e^2} \right)$$
$$- K_i \exp\left(-\frac{(SF - \mu_i)^2}{2\sigma_i^2} \right),$$
(9)

where $R_0, K_e, \mu_e, \sigma_e, K_i, \mu_i$ and σ_i are parameters to be determined, and SF represents the variable of spatial frequency. The fitting procedure is to search for the best parameters $R_0, K_e, \mu_e, \sigma_e, K_i, \mu_i$ and σ_i so that the fitting curve has the least square error with the given spatial frequency tuning curve. Having determined the parameters, one can identify the optimal spatial frequency (SF_{op}) of the fitting curve. Then the second step is to calculate the value of variance at low spatial frequencies, the LSFV, according to the formula:

$$LSFV[R] = \frac{\int_{SF_{op}/M}^{SF_{op}} R(SF) \big(log_M(SF) - log_M(SF_{op}) \big)^2 dlog_M(SF)}{\int_{SF_{op}/M}^{SF_{op}} R(SF) dlog_M(SF)},$$
(10)

where M refers to the number of data points, which are evenly spaced in log spatial frequency. In this work, as

in (Xing et al. 2004), M is set to be 16. Therefore, LSFV considers the left branch of the spatial frequency tuning

curve from 1/16 of the optimal spatial frequency to the optimal spatial frequency. The smaller the LSFV the more attenuating at the optimal spatial frequency, and the more tuned for spatial frequency.

2.5 Numerical implementation

With a large-scale network model, the most important issue of numerical implementation is how to calculate exactly and efficiently the cortical-cortico excitations/inhibitions that arise in the model V1 layer. In the following, we focus on this issue. Other parts of the numerical implementation can be carried out in standard ways.

We first discuss the case when the synaptic filter's impulse response function $G_E(t)$ takes the form Eq. (5). For the simplicity of presentation, we consider the following generic form:

$$\mathbf{G}_E(t) = t^n e^{-t} H(t). \qquad (11)$$

Our goal is to calculate $\sum_k a_{j-k} \sum_m G_E(t - t_m^k)$ exactly and efficiently. To this end, we introduce the following notations:

$$g^j(t) = \sum_k a_{j-k} \sum_m G_E\left(t - t_m^k\right),$$

$$s_p^j(t) = \sum_k a_{j-k} \sum_m G_p\left(t - t_m^k\right), \qquad (12)$$

where $G_p(t) = t^{n-p} \exp(-t)$, $p = 1, ..., n$. In fact, the conductance $g^j(t)$ represents the cortical-cortico excitation/inhibition received by the jth neuron at time t.

If there are no spikes during the time interval $[t_l, t_l + dt]$ over the network, where dt is the time step size and $t_l = l * dt$, direct calculation shows that:

$$g^j(t_l + dt) = \sum_k a_{j-k} \sum_m \left(t_l + dt - t_m^k\right)^n e^{-\left(t_l + dt - t_m^k\right)}$$

$$= e^{-dt} \sum_k a_{j-k} \sum_m$$

$$\times \left[\sum_{p=0}^n \mathbf{C}_n^p dt^p \left(t_l - t_m^k\right)^{n-p} e^{-\left(t_l - t_m^k\right)} \right]$$

$$= e^{-dt} \sum_{p=0}^n \left[\sum_k a_{j-k} \sum_m \mathbf{C}_n^p dt^p \right.$$

$$\left. \times \left(t_l - t_m^k\right)^{n-p} e^{-\left(t_l - t_m^k\right)} \right]$$

$$= e^{-dt} \left[g^j(t_l) + \sum_{p=1}^n \mathbf{C}_n^p dt^p s_p^j(t_l) \right], \qquad (13)$$

where $\mathbf{C}_n^p = \frac{n!}{p!(n-p)!}$, and

$$s_p^j(t_l + dt) = e^{-dt} \left[s_p^j(t_l) + \sum_{q=1}^{n-p} \mathbf{C}_{n-p}^q dt^q s_{q+p}^j(t_l) \right],$$

$$p = 1, ..., n. \qquad (14)$$

When there is a spike during the interval $[t_l, t_l + dt]$ in the ith neuron, then a conductance increment should be propagated to the jth neuron, which leads to the new form of g^j and s_p^j as follows:

$$g^j(t_l + dt) = e^{-dt} \left[g^j(t_l) + \sum_{p=1}^n \mathbf{C}_n^p dt^p s_p^j(t_l) \right]$$

$$+ a_{j-i} \left(t_l + dt - t^*\right)^n e^{-(t_l + dt - t_*)}, \qquad (15)$$

and

$$s_p^j(t_l + dt) = e^{-dt} \left[s_p^j(t_l) + \sum_{q=1}^{n-p} \mathbf{C}_{n-p}^q dt^q s_{q+p}^j(t_l) \right]$$

$$+ a_{j-i} \left(t_l + dt - t^*\right)^{n-p} e^{-(t_l + dt - t_*)},$$

$$p = 1, ..., n, \qquad (16)$$

where $t^* \in [t_l, t_l + dt]$ is the time of the spike.

Similarly, we can derive a similar formula when the synaptic filter's impulse response function $G_E(t)$ takes the form Eq. (8) (not shown).

The method is exact since no approximation is introduced. Moreover, it is also very efficient. In fact, in the case when there are no spikes over the network during the time interval $[t_l, t_l + dt]$, the cortical-cortico excitations/inhibitions at the time $t_l + dt$ can be efficiently calculated by Eqs. (13) and (14), which only involve $O(N)$ numerical operations with N being the number of neurons in the network. In the generic case when spikes occur over the network, the method is also efficient. Note the fact that the spike rates of V1 neurons range from 0 to several hundreds, which means that in many time intervals $[t_l, t_l + dt]$, a V1 neuron will be silent. This implies that the advance of the cortico-cortical conductance for each V1 neuron is mainly implemented by Eq. (13).

3 Results

In this paper, the visual stimuli considered are drifting gratings. As discussed before, these stimuli are often used in experiments on orientation and spatial frequency selectivity in V1. We test our model under 64 experimental conditions, by applying stimuli with 8 orientations ($\theta = \frac{m\pi}{4}$, $m = 0, ..., 7$) and 8 spatial frequencies ($k = 2^n$cycles/degree, $n = -4, ..., 3$) and with the highest
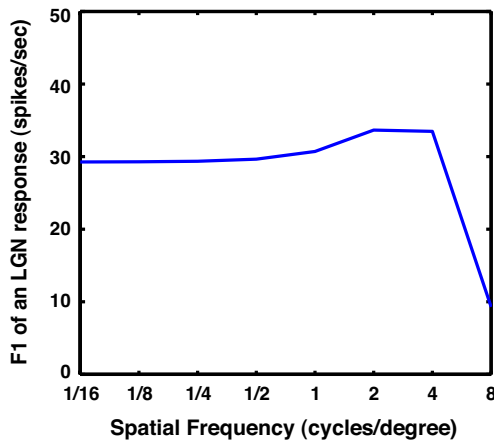
Fig. 2 Tuning curve of the model's LGN cell response (F1 component) w.r.t. spatial frequency. The LSFV for this model neuron is 1/3, and its CV=1

contrast ($\epsilon = 1.0$). For each model neuron, the preferred orientation and preferred spatial frequency are taken to be those values where the spike rate is highest among the 64 simulated experiments. Cells were classified into simple and complex groups as previously (Tao et al. 2004) to facilitate comparisons with published experimental data, though we know there is a continuum of intracellular properties (Mechler and Ringach 2002; Priebe et al. 2004; Tao et al. 2004).

As in experiments, we exclude cells that are firing weakly from further analysis . The criterion we used was 8 spikes/s. If the maximum response a cell produced to all 64 stimuli was below criterion, it was excluded from the population analysis, as we have done in population data analysis of experimental data (Ringach et al. 2002a). Approximately one third of the excitatory cells were excluded from further analysis on the basis of the response criterion. As far as we know, there are no experimental data on the fraction of weakly firing cells.

3.1 Spatial frequency preference and selectivity

The spatial frequency tuning curve of the LGN cells in the model is shown in Fig. 2. This follows from the spatial kernel $A(x)$ of an LGN cell given in Methods above, and is an approximation to measurements of the spatial frequency responses of macaque magnocellular LGN cells (Derrington and Lennie 1984). The tuning curve is broad with a peak around 3c/deg. The LSFV value for this cell is 1/3 because it is so broadly tuned and low-pass.

To try to understand the mechanisms that produce spatial-frequency-selective responses in our model, we select two representative model V1 neurons: one simple cell and one complex cell. Figure 3 displays the spatial frequency tuning curves of the cycle-averaged

Fig. 3 Tuning curves of firing rates with respect to spatial frequencies and cycle-averaged firing rates (with the spontaneous rate in *red*) for all the eight spatial frequencies. The *plots in the first row* are for the simple cell at location (39, 33) in the model while those in the *second row* for the complex cell at (83, 91). Also for the simple cell we plot the peak deviation vs spatial frequency for the summed LGN current
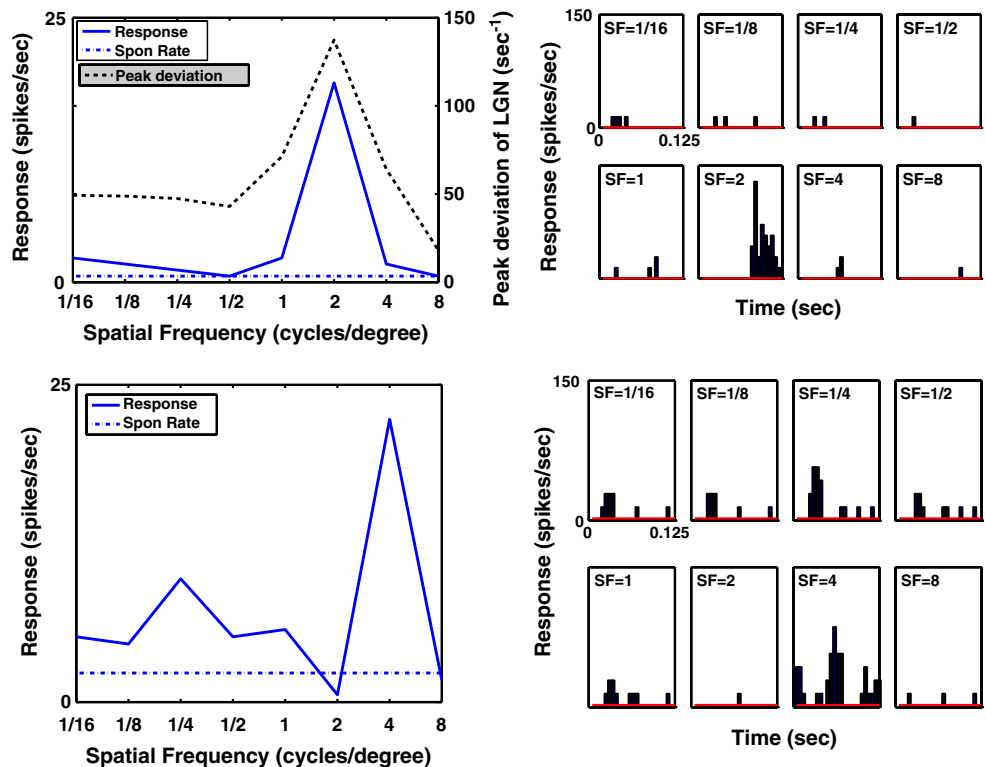
firing rate for the two example neurons. Compare how sharply tuned they are compared to individual LGN neurons as in Fig. 2. To visualize the input-output transformation of spatial frequency signals, we also plot on the same spatial frequency axis the peak deviation of the summed input current from all LGN-cortical synapses onto the simple cell, as an indication of the tuning of the summed feedforward input. The responses of both of the two example neurons are greatly suppressed at low spatial frequency compared to the response of a single LGN cell as in Fig. 2. The simple cell's tuning curve is also suppressed below that of the peak deviation of the summed LGN input that converges on this cortical cell, which might provide a clue that LGN input could not fully explain the selectivity for spatial frequency and inhibition is also another main source for the selectivity.

The suppression of responses at spatial frequencies below the peak spatial frequency is caused by the inhibition in the network. The inhibition is induced by the activity of inhibitory neurons. The more active the inhibitory neurons are the stronger the inhibition is. To check the activity of inhibitory neurons, we randomly select one model inhibitory neuron, whose spatial frequency tuning curve was graphed in Fig. 4. The response of this inhibitory neuron at low spatial frequency is much stronger than those of the two excitatory neurons in Fig. 3. Indeed, note that with the conductance coupling matrix we used for the network, the self-inhibitory coupling of inhibitory neurons $S_{II} = 65.0 < S_{EI} = 80.0$. This inequality explains the larger responses of inhibitory neurons in contrast to that of excitatory neurons. It is this strong inhibition that suppresses the responses of excitatory neurons at low spatial frequencies, which subsequently sharpens the selectivity for spatial frequency. This modeling result is consistent with the hypothesis offered by Ringach et al. (2002b) and Bredfeldt and Ringach (2002) about

the role of cortical suppression in explaining their results on the dynamics of spatial frequency selectivity. We'll consider further the consequences of the different patterns of spatial frequency tuning in inhibitory and excitatory neurons below when we discuss the spatial frequency dependence of intracellular response components.

3.2 Time courses of intracellular responses in the model

We next examine the time courses of intracellular response variables of the two model excitatory neurons in Fig. 5. The time courses make clearer how the cortex is increasing spatial frequency selectivity by suppressing responses to non-preferred stimuli. The figure shows the two neurons' cycle-averaged LGN excitatory conductances, cortically-driven excitatory conductance, inhibitory conductances, and effective reversal potentials V_S. Each of these four intracellular variables is plotted in eight separate plots depicting responses at the eight spatial frequencies at each neuron's preferred orientation.

As seen in the averaged responses in Fig. 5, the LGN excitatory input to the simple cell is much larger than to the complex cell. Cortico-cortical excitation compensates for the difference in strengths between the two LGN inputs. Inhibitory conductance is almost at the same level for these two example neurons though as shown later there is some variation in mean inhibition across the population, and this variation is probably functionally significant.

Many simple cell candidates (roughly speaking, V1 neurons that receive more than 15 LGN inputs), like the representative simple cell shown, have low spike rates at low spatial frequencies and thus evoke weak excitatory postsynaptic conductances in complex cell

Fig. 4 Tuning curves of firing rates with respect to spatial frequency, and cycle-averaged firing rates (with the spontaneous rate in *red*), for an inhibitory neuron at location (50, 48) in the model
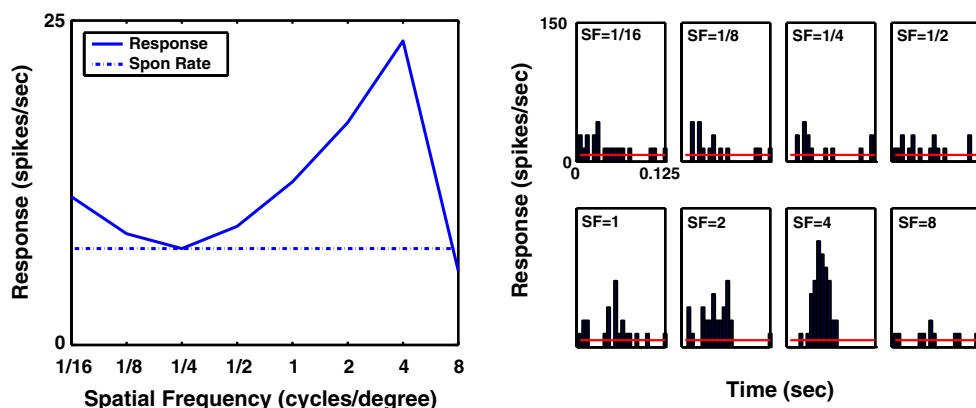
Fig. 5 Cycle-averaged LGN input, cortico-cortical excitation, inhibition and effective reversal potential for two model neurons for eight spatial frequencies at their own preferred orientation (with the corresponding values of the spontaneous rate in *red*). The plots in the *left column* are for the simple cell located at (39, 33) while the plots in the *right column* are for the complex cell at (83, 91) in our 128×128 neuronal network
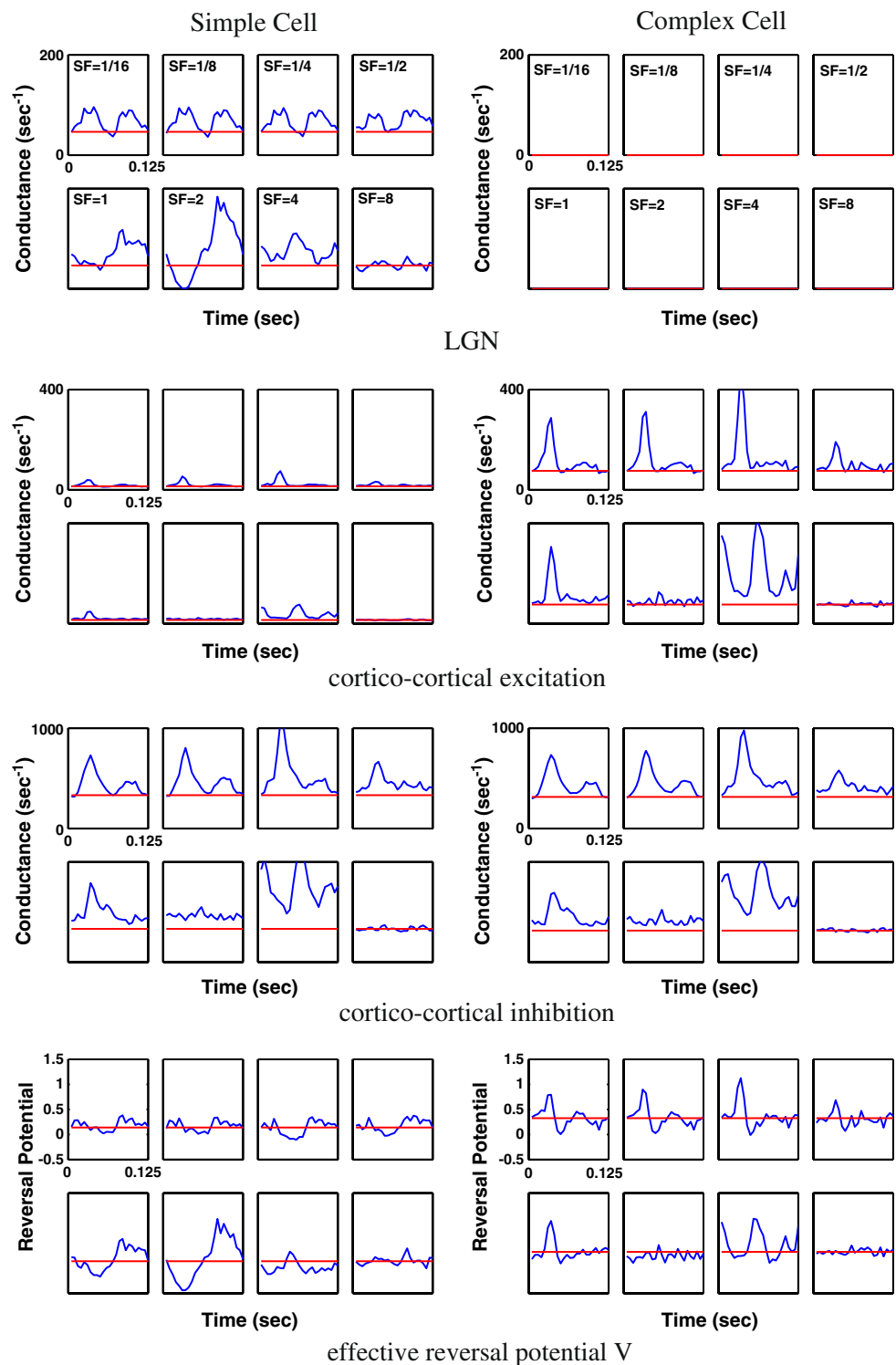
candidates (roughly speaking, the model neurons that receive less than 15 LGN inputs). Therefore, the network is in a low firing state in response to low spatial frequency (sf<0.5 c/deg). However, as spatial frequency increases, many simple cell candidates fire at their preferred spatial frequencies, inducing stronger excitatory postsynaptic conductance in the complex cell candidates, thus causing the network to have a high firing state. Suppressed by the strong inhibition in the network, only well-modulated simple cell candidates, and those complex cell candidates receiving strong cortical excitation, can fire.

One might still ask, why are the simple cells' responses to low spatial frequencies so much worse than in the LGN input? One can observe this is the case by examining the low spatial frequency range in Fig. 3 and comparing it to the LGN excitation at low spatial frequency on the simple cell in Fig. 5. The explanation for the difference between the excitatory conductance and the cell's spike rate function can be found in the responses of inhibition in Fig. 5 across spatial frequency, and also in the spatial frequency response of individual inhibitory neurons, one of which is shown in Fig. 4. The responses of inhibitory neurons decline at low spatial frequencies but not as much as for the excitatory neurons. One can see this point by gauging the magnitude of inhibition's response at low spatial frequency in Fig. 5, or by comparing the histogram of LSFV for inhibitory and excitatory neurons in Fig. 8. Especially, for the histograms of LSFV in Fig. 8, one can find that there is a shift to right for inhibitory neurons relative to excitatory neurons. Based on the definition of LSFV, this means that inhibitory neurons are generally more active than excitatory neurons at low spatial frequencies. Thus, inhibitory neurons provide strong inhibition across a broad range of spatial frequencies and this inhibition suppresses the low spatial frequency responses of the excitatory neurons in the model.

Note also the temporal waveform of responses in the summed LGN input to simple cells at low spatial frequencies in Fig. 5. The LGN input is frequency doubled, meaning there are two excitatory peaks for each temporal cycle of drift. The reason for the frequency doubling is straightforward; it is the spike threshold in individual LGN cells. Low spatial frequency stimuli excite first the ON cells, then the OFF cells for each cycle of drift, and the two waves of excitation converge onto a cortical cell each drift cycle. However, the model simple cell's membrane potential, which is approximately equal to the effective reversal potential V_S in Fig. 5, will show little frequency doubling because of synaptic inhibition that quenches it, in analogy to what happened in Wielaard et al. (2001). In the Discussion we return to the frequency doubling and how it might be used to test the model.

3.3 Spatial frequency selectivity across the V1 population

Figure 6 is a summary figure that shows numerical results about the distribution of preferred spatial frequency across the population of excitatory and inhibitory neurons in the model. The preference plot demonstrates that the preferred spatial frequencies mainly concentrate in the middle of the spatial
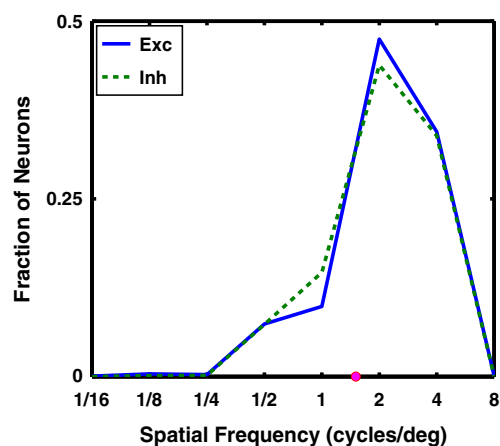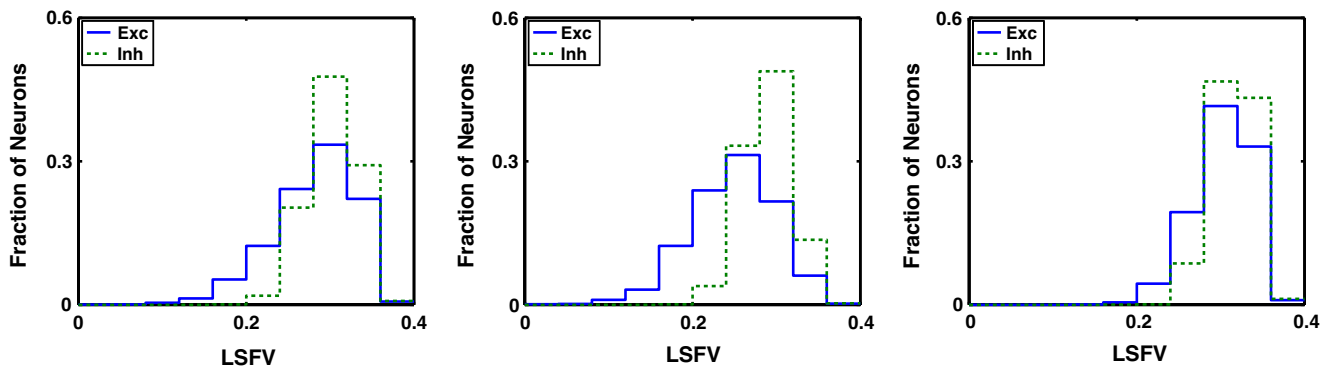

Fig. 6 Distribution of preferred spatial frequency in the model. The *dashed curve* is for the population of inhibitory neurons and the *solid curve* is for excitatory neurons. The *red dot* represents the peak of the spatial frequency tuning curve for an LGN cell

frequency range we studied, and this distribution corresponds very well with V1 measurements (DeValois and DeValois 1988). The red dot on the x-axis corresponds to the preferred spatial frequency of a single LGN cell. In the model all the LGN cells have the same spatial frequency preference. The solid curve is the population distribution of spatial frequency preferences for excitatory cells, while the dashed curve is for inhibitory cells in the model. The preference curves for the model's excitatory and inhibitory populations are nearly the same. Based on our many simulations with different sets of cortico-cortical conductance parameters , we concluded that the model's matching of the spatial frequency preference distribution of the real cortex is not a trivial result, and is not simply a consequence of the LGN
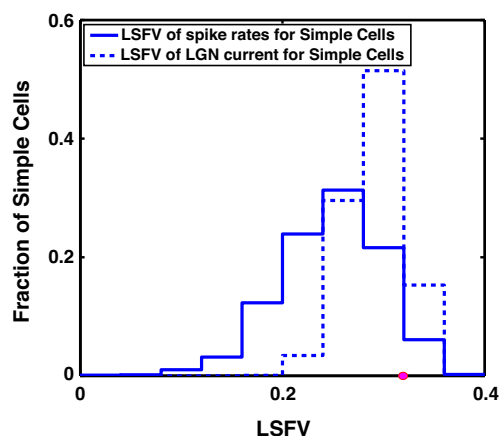
Fig. 7 Comparison of low spatial frequency variances (*LSFV*) of spike rates and LGN current for simple cells. The *red dot* represents the LSFV for an LGN cell

Fig. 8 The distributions of LSFV for all neurons (*left*), simple cells (*middle*) and complex cells (*right*). The plots demonstrate that LSFV is broadly distributed for excitatory neurons and also that simple cells are better tuned than complex cells. In each panel, the *dashed histogram* is for the population of inhibitory neurons and the *solid curve* is for excitatory neurons

input patterns onto simple cells. The spatial frequency preference of model neurons is affected significantly by the connectivity matrix and by the locations of the neurons in the model network.

The transformation of spatial frequency tuning across the population of V1 simple cells in the model is illustrated in Fig. 7. This figure shows the distribution of the LSFV measure for simple cell firing rates as the solid histogram, and for the summed LGN current to each neuron as the dashed histogram. It is evident that the firing rate histogram, the result of the cortical computation, is shifted to the left, meaning lower average LSFV, meaning higher spatial frequency selectivity for cortical simple cells compared to their LGN inputs.

The responses of excitatory cells are suppressed at spatial frequencies above and below the peak spatial frequency (Fig. 7). This might be explained broader tuning in inhibitory neurons in the model. The increased breadth of inhibitory tuning is illustrated in

Fig. 8 where the LSFV's of excitatory and inhibitory neurons are compared. Across the entire model V1 population and also in the subset of simple cells, the LSFV of inhibitory neurons is markedly less spatial-frequency-selective as indicated by the rightward shift of the LSFV distribution to higher LSFV values, meaning less selectivity, for inhibitory neurons. Why does this difference happen between excitatory neurons and inhibitory neurons? As discussed before, although there is no much difference for their received excitation (including LGN inputs and external noise), the excitatory and inhibitory neurons obtain saliently different amount of inhibition, which is mainly embodied by the coupling matrix with $S_{II} = 65 < S_{EI} = 80$ in our network model. Therefore, the weaker inhibition received
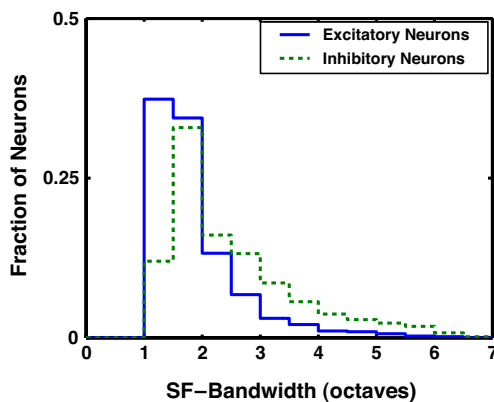

Fig. 9 Histogram of spatial frequency bandwidth for excitatory neurons (*solid-line histogram*) and inhibitory neurons (*dashed-line histogram*)
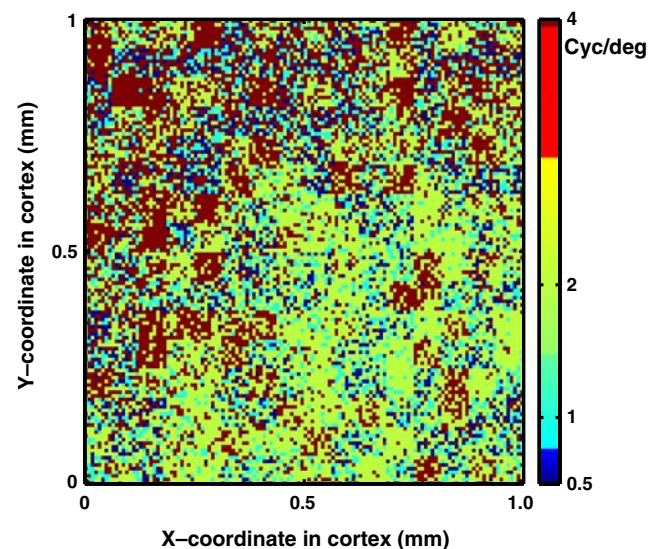
Fig. 10 Spatial distribution of the preferred spatial frequency across the cortical surface in the model

Fig. 11 The averaged conductance vs LSFV. The plots in the *top row* represent the averaged inhibition as functions of LSFV for simple cells (*left*) and complex cells (*right*) respectively. The plots in the bottom row are for the averaged excitation. In these figures, the averaged conductance is averaged over all eight orientations and all eight spatial frequencies
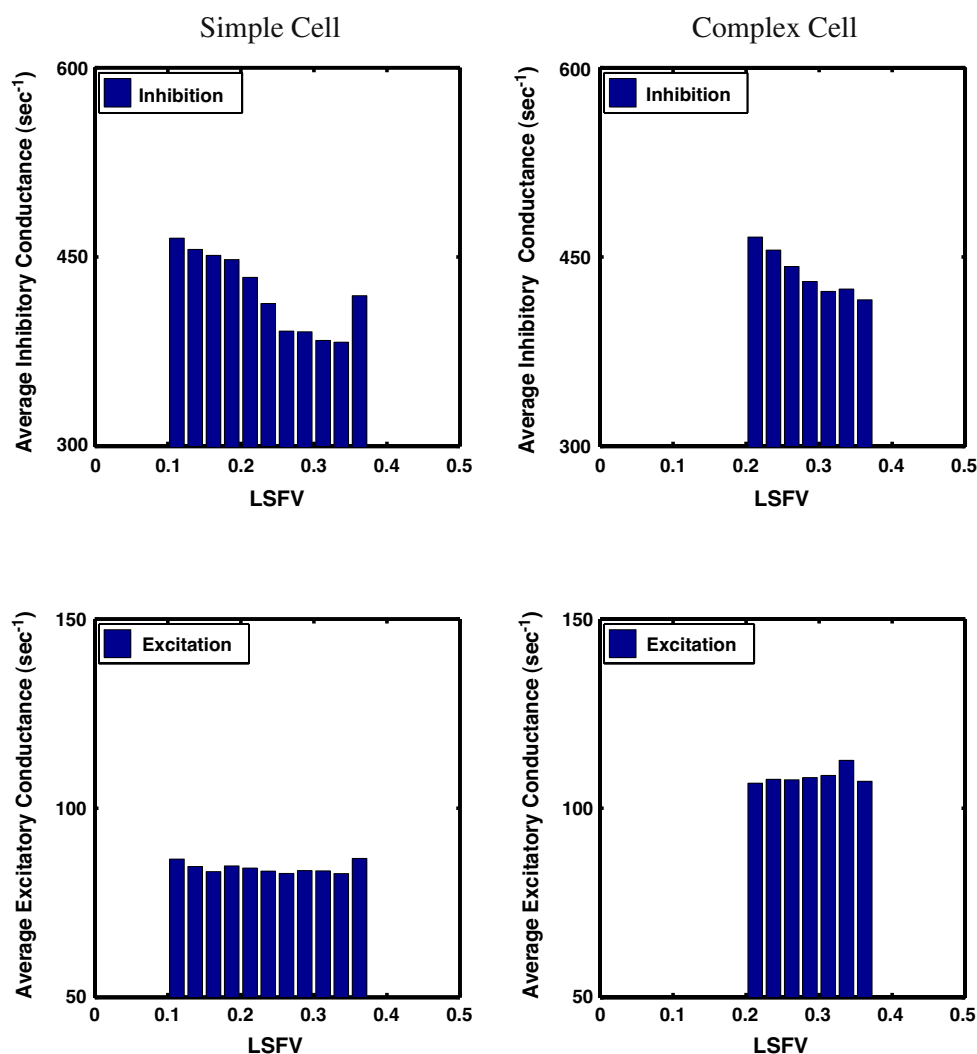
by inhibitory neurons yields the broader tuning for spatial frequency.

A conventional measure of spatial frequency tuning is the bandwidth. As a further test of the model's performance, we show the population distribution of spatial frequency bandwidth of the model in Fig. 9. The model's bandwidth distribution for excitatory neurons is similar to what has been reported for V1 (e.g., DeValois and DeValois 1988). Inhibitory neurons in the model systematically have larger bandwidths than excitatory neurons.

It is of interest to study the map of spatial frequency preference across the model population. We examined a map of peak spatial frequency across the cortical layer in Fig. 10. Spatial frequency preference is not spatially organized in the present model, in agreement with experimental evidence about the spatial distribution of spatial frequency preference (Sirovich and

Uglesich 2004). The random arrangements of clusters (see Methods) caused a very non-uniform distribution of preferred spatial frequency as shown in Fig. 10. We tested several different random distributions of receptive field clusters with different random seeds, and all results presented in this paper were robust.

3.4 Synaptic conductances and spatial selectivities

Studying the correlation of spatial selectivity with amount of synaptic inhibition across the neuronal population, is a way to test whether inhibitory strength controls selectivity. Figure 11 shows the relation between strengths of inhibitory and excitatory synaptic conductances and the spatial frequency LSFV for simple and complex cells. Higher amounts of synaptic inhibition are associated with lower LSFV (more spatial

Fig. 12 The histograms of cycle-averaged spike rate in responses to the optimal stimulus for the excitatory neurons (*top left*), the inhibitory neurons (*top right*), the simple cells (*bottom left*) and the complex cells (*bottom right*)
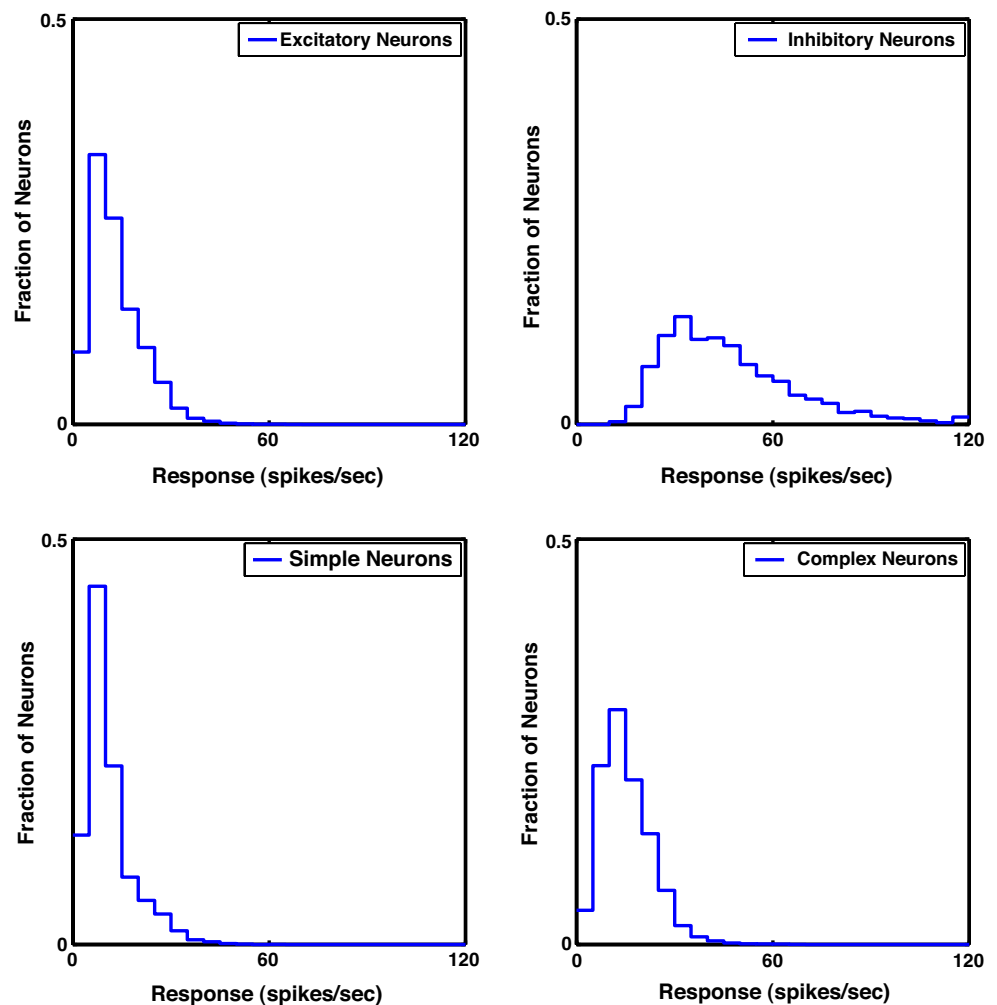
frequency selectivity) and this effect is present for both simple and complex cells. There appears to be no consistent relation between excitatory conductance strength and LSFV for either simple or complex cells. Synaptic conductance strengths in the model can vary because of location within the layer of V1, because of variations in the total amount of cortical input from neighboring neurons. What Fig. 11 indicates is that the variation of inhibitory synaptic strength causes diversity in spatial frequency selectivity.

3.5 Spike firing rates in the model neuron population

The model allows us to compare neuronal activity levels across the population of model neurons in the input layer. To assess the biological realism of the model, it is worth comparing the peak spike firing rates to optimal visual stimuli in different types of model neurons. Results of such comparisons are shown in

Fig. 12. Two different comparisons are made in the figure, between excitatory and inhibitory cells (upper row) and between excitatory cells classified as simple and excitatory cells classified as complex (lower row). Based on the responses to optimal stimuli, the firing rate distributions are quite different between the excitatory cells as a whole and the inhibitory cells. The inhibitory cells in the model fire spikes at much higher rates on the average than excitatory cells. This is a consequence of the synaptic coupling matrix we chose to use to account for the spatial selectivity of the real V1 cortex. Between simple and complex cells there is much less of a difference as seen in Fig. 12. But there is a tendency for the complex cells to produce higher firing rates in response to their optimal stimuli than simple cells do. The fraction of simple cells with very low firing rate responses is higher than for complex cells. The differences in firing rates may reflect the balance between excitation and inhibition that causes the cells to be classified as simple or complex. These firing rate

distributions are predictions of the model that can be compared with data from real V1.

4 Discussion

4.1 Inhibition and spatial selectivities

A major result of this paper is the importance of the role of cortical inhibition or suppression in the dynamics of this neuronal network model. The results in this paper illustrate the effect of strong inhibition in suppressing V1 neurons' responses to stimuli with low spatial frequencies. Specifically, similar to orientation preference, spatial frequency preference arises when V1 neurons receive synaptic drive from LGN. The strong inhibition in the network suppresses V1 neurons' responses, and this makes V1 neurons fire very few spikes to non-preferred stimuli. This is the reason in the model for V1 neurons' narrow tuning for spatial frequency (cf. Lauritzen and Miller 2003).

A similar mechanism makes the model's neurons orientation-selective. As in previous neuronal models (Troyer et al. 1998; McLaughlin et al. 2000; Wielaard et al. 2001; Tao et al. 2004), in this model strong cortical inhibition sharpens orientation selectivity (Zhu et al., manuscript in preparation).

The sharpening of spatial frequency tuning by nonlinear suppression as a result of cortical inhibition is a different mechanism from what has been proposed previously as an explanation for the genesis of cortical spatial frequency tuning (summarized in DeValois and DeValois 1988). The usual explanation for heightened spatial frequency selectivity in the cortex has been feedforward convergence of LGN cells onto V1 cells, and then more feedforward convergence of V1 cells onto higher-level V1 cells–to create receptive fields with multiple sub-regions that will make neurons more spatial-frequency selective. But in our model the LGN input to a V1 neuron is only into two or three subregions, and the very highly selective neurons become selective not by feedforward convergence but because of nonlinear suppression by inhibition. This idea is similar to what was proposed from experimental results on the time-evolution of spatial frequency selectivity (Bredfeldt and Ringach 2002; Ringach et al. 2002b).

In response to a reviewer, we performed computational experiments to reinforce our conclusions. When the inhibition in the model is turned off, all neurons fire at the maximum spike rates constrained only by the refractory period. This experiment supports the idea that inhibition plays a crucial role in suppressing neurons' activity. For the second experiment when all

V1 neurons share the same width of their receptive fields (suppose all widths are set to be 2, corresponding to 2 cycles/degree), the model is very similar to the original Egalitarian model (Tao et al. 2004) except that our present model incorporates 50% sparsity of connections. The experiment with the same coupling parameters as in our present model shows: a) too many complex cells (in contrast to simple cells), b) unrealistically large spike rates for many V1 neurons, c) the histogram of preferred spatial frequency takes large values at some low spatial frequencies. We also tried another experiment with a smaller value of the maximum of S_{EE}, which leads to weak cortico-cortical excitation. We found: a) not many complex cells (in contrast to simple cells), b) the histogram of preferred spatial frequency mainly focuses at 2 cycles/degree. These two experiments demonstrate the bi-stability phenomenon discussed in (Cai et al. 2004) and more importantly show that the spatial pattern of LGN inputs also plays a crucial role in spatial frequency selectivity.

4.2 Comparisons with other models

In this work we present a new neuronal network model of primary visual cortex. Our model reproduces many aspects of real data, including orientation selectivity and simple/complex cells. Specifically, the way this model produces simple/complex cells is identical to that of the Egalitarian model (Tao et al. 2004): V1 neurons receive roughly the same amount of excitatory postsynaptic drive divided between LGN input and cortico-cortical excitations. Those model neurons that receive a large amount of LGN input become simple cells while those that receive large amounts of cortico-cortical excitation become complex cells.

The novelty of our model is that it can explain results on spatial frequency selectivity. To accomplish this, instead of assigning each V1 model neuron the same width of receptive field, our model introduces variability of those widths. This new structure makes it possible for V1 neurons to be sensitive to different spatial frequencies, thus introducing diversity of spatial frequency preference resembling the real V1 (DeValois and DeValois 1988).

Moreover, the introduction of width-variability makes the present model more robust than the Egalitarian model. As discussed in (Cai et al. 2004), if cortico-cortical excitation in the Egalitarian model (Tao et al. 2004) is increased too much, there is a bistability in the network with complex cells firing either too much or too little. As demonstrated theoretically by Cai et al. (2004), sparsity of cortico-cortical connections allows cortico-cortical excitation to be stronger before

the bi-stability regime is reached. The Egalitarian model (Tao et al. 2004) produced simple cells with good orientation selectivity but most complex cells in that model were not very orientation-selective. Following the analysis of Cai et al. (2004), the sparse coupling in the modified Egalitarian model of Tao et al. (2006) enabled greater cortico-cortical excitation that produced more selective complex cells. The present model achieves some effective sparsity as a consequence of the spread of spatial frequency preferences. Indeed, due to the variability in width of V1 neurons' receptive fields as well as the strong inhibition among cells in our network, many V1 neurons fire very few spikes or even are silent in response to an ineffective stimulus with the "wrong" spatial frequency. Nevertheless, the effective sparsity was not enough to achieve a distribution of spatial frequency selectivity like the real cortex's, and we had to introduce sparsity into the model, as described in Methods and Results. We only needed sparse coupling between excitatory neurons and all the other neurons, consistent with experimental results (Holmgren et al. 2003; but see Yoshimura and Callaway 2005). However, in contrast to the model in Tao et al. (2006), the intrinsic effective sparsity of our model relaxes the strict requirement of the degree of sparsity.

Recently Finn et al. (2007) have revived the feedforward model to try to explain orientation selectivity. Specifically, they report that contrast-invariant orientation selectivity can be observed in a model that includes no inhibition but that does have a high spike threshold and variability in the membrane potential. With respect to the importance of noise and threshold, our model agrees with Finn et al. (2007)'s results in that spikes in our model are evoked mostly by fluctuations in the membrane potential that are a result of randomness in LGN spike firing and in the cortico-cortical input that we called "external noise". In this way the present model resembles the simple cell model of Wielaard et al. (2001) in which neurons fired spikes only when noise fluctuations caused the effective reversal potential V_S to exceed 1, the normalized threshold (Shelley et al. 2002). However, above we showed that high selectivity for spatial frequency was correlated with high values of inhibitory conductance, in Fig. 11. This theoretical result parallels experimental results that indicate that orientation selectivity is markedly reduced by weakening intracortical inhibition (Sato et al. 1996). Therefore one test of our model is to test a strong prediction of the model: that blocking local, cortical inhibition should markedly reduce spatial frequency selectivity. This would also test Finn et al.'s (2007) modified feedforward model that makes the opposite prediction. Another test of our model involves the frequency doubling of LGN input at low spatial frequency in simple cells as seen in Fig. 5. Our model predicts that low spatial frequency responses of V1 simple cells, recorded intracellularly, should not have much frequency doubling in the membrane potential but may have large frequency doubling of conductance (both total and excitatory). Feedforward models without synaptic inhibition would predict as much frequency doubling in the membrane potential as we show in the LGN conductance in Fig. 5. This is another clearly testable difference in the predictions of the two models.

4.3 Modeling considerations

One important area where we had to make a choice in the model is about how spatial frequency preference or bias, induced from the LGN input, is organized spatially in the input to the model. There is controversy in the literature on this. The idea of random clusters is our interpretation of the optical imaging paper about spatial frequency maps in V1 by Sirovich and Uglesich (2004). Completely different optical imaging maps have been reported by others (Issa et al. 2000). Our judgment was that the quasi-random clustering of spatial frequency bias deduced from the maps in Sirovich and Uglesich (2004) made the most sense in terms of the physiological recording literature (DeAngelis et al. 1999). Also, Xing et al. (2004) comment that there appears to be little correlation between preferred spatial frequency and orientation selectivity assessed by CV, and this result also made us believe the more random maps suggested by Sirovich and Uglesich (2004). The resulting model does account for correlations between spatial selectivities in a way that makes the choice we made seem reasonable, but further experiments and modeling will be needed to validate this choice.

In large computational models there are many parameters and it may be difficult to judge as a reader what is constrained and what if anything is indeterminate in a large-scale model like the one we offer here. One advantage of making a model of V1 compared to making models of other cortical areas is that many model parameters are constrained, either directly or indirectly, by data about V1 responses to visual stimuli. Also much is known about the distributions of spatial frequency and orientation selectivity across the V1 population, and also about the F_1/F_0 ratio in V1. Synaptic time courses also are pre-determined by previous data. What are malleable and what are challenges for the modeler are the values of the synaptic couplings and their relative strength compared to each other. What we do not show but what took most of the work for this paper is the exploration of different

values of the ratio S_{EE}/S_{EI}. We know that if S_{EI} is too weak in the model, there are not enough simple cells. This theoretical finding echoes some interesting physiological results that the classification of a cell as simple or complex can be changed by manipulation of cortical inhibition (Murthy and Humphrey 1999; Bardy et al. 2006). Also, neuropharmacological weakening of inhibition also reduces selectivity for orientation, measured globally (Sato et al. 1996). These experimental results support the concept of the model. The many results about spatial selectivity shown in the Results section that agree well with cortical experimental data also support the large-scale V1 model.

References

Bardy, C., Huang, J. Y., Wang, C., FitzGibbon, T., & Dreher, B. (2006). 'Simplification' of responses of complex cells in cat striate cortex: Suppressive surrounds and 'feedback' inactivation. *Journal of Physiology, 574*, 731–750.

Beierlein, M., Gibson, J. R., & Connors, B. W. (2003). Two dynamically distinct inhibitory networks in layer 4 of the neocortex. *Journal of Neurophysiology, 90*, 2987–3000.

Bredfeldt, C. E., & Ringach, D. L. (2002). Dynamics of spatial frequency tuning in macaque V1. *Journal of Neuroscience, 22*, 1976–1984.

Cai, D., Tao, L., Shelley, M., & McLaughlin, D. (2004). An effective kinetic representation of fluctuation-driven neuronal networks with application to simple and complex cells in visual cortex. *Proceedings of the National Academy of Science of the United States of America, 101*, 7757–7762.

Campbell, F. W., Cooper, G. F., & Enroth-Cugell, C. (1969). The spatial selectivity of the visual cells of the cat. *Journal of Physiology, 203*, 223–235.

Chance, F. S., Nelson, S. B., & Abbott, L. F. (1999). Complex cells as cortically amplified simple cells. *Nature Neuroscience, 2*(3), 277–282.

Dayan, P., & Abbott, L. (2001). *Theoretical neuroscience.* Cambridge: MIT.

DeAngelis, G., Ohzawa, I., & Freeman, R. D. (1995). Receptive-field dynamics in the central visual pathways. *Trends in Neuroscience, 18*, 451–458.

DeAngelis, G. C., Ghose, G. M., Ohzawa, I., & Freeman, R. D. (1999). Functional micro-organization of primary visual cortex: Receptive field analysis of nearby neurons. *Journal of Neuroscience, 19*, 4046–4064.

Derrington, A. M., & Lennie, P. (1984). Spatial and temporal contrast sensitivities of neurones in lateral geniculate nucleus of macaque. *Journal of Physiology, 357*, 219–240.

DeValois, R. L., Albrecht, D. G., & Thorell, L. G. (1982). Spatial frequency selectivity of cells in macaque cortex. *Vision Research, 22*, 545–549.

DeValois, R. L., & DeValois, K. K. (1988). *Spatial vision.* New York: Oxford University Press.

Enroth-Cugell, C., & Robson, J. (1966). The contrast sensitivity of retinal ganglion cells of the cat. *Journal of Physiology, 187*, 517–552.

Finn, I. M., Priebe, N. J., & Ferster, D. (2007). The emergence of contrast-invariant orientation tuning in simple cells of cat visual cortex. *Neuron, 54*, 137–152.

Gibson, J., Beierlein, M., & Connors, B. (1999). Two networks of electrically coupled inhibitory neurons in neocortex. *Nature, 402*, 75–79.

Holmgren, C., Harkany, T., Svennenfors, B., & Zilberter, Y. (2003). Pyramidal cell communication within local networks in layer 2/3 of rat neocortex. *Journal of Physiology, 551*, 139–153.

Hubel, D. H., & Wiesel, T. N. (1962). Receptive fields, binocular interaction and function architecture in the cat's visual cortex. *Journal of Physiology, 160*, 106–154.

Issa, N. P., Trepel, C., & Stryker, M. P. (2000). Spatial frequency maps in cat visual cortex. *Journal of Neuroscience, 20*, 8504–8514.

Koch, C. (1999). *Biophysics of computation.* Oxford: Oxford University Press.

Kuffler, S. K. (1953). Discharge patterns and functional organization of mammalian retina. *Journal of Neurophysiology, 16*, 37–68.

Lauritzen, T. Z., & Miller, K. D. (2003). Different roles for simple-cell and complex-cell inhibition in V1. *Journal of Neuroscience, 23*(32), 10201–10213.

McLaughlin, D., Shapley, R., Shelley, M., & Wielaard, J. (2000). A neuronal network model of sharpening and dynamics of orientation tuning in an input layer of macaque primary visual cortex. *Proceedings of the National Academy of Science of the United States of America, 97*, 8087–8092.

Mechler, F., & Ringach, D. L. (2002). On the classification of simple and complex cells. *Vision Research, 42*, 1017–1033.

Movshon, J. A., Thompson, I. D., & Tolhurst, D. J. (1978). Spatial and temporal contrast sensitivity of neurons in areas 17 and 18 of the cat's visual cortex. *Journal of Physiology, 283*, 101–120.

Murthy, A., & Humphrey, A. L. (1999). Inhibitory contributions to spatiotemporal receptive-field structure and direction selectivity in simple cells of cat area 17. *Journal of Neurophysiology, 81*, 1212–1224.

Priebe, N. J., Mechler, F., Carandini, M., & Ferster, D. (2004). The contribution of spike threshold to the dichotomy of cortical simple and complex cells. *Nature Neuroscience, 7*, 1113–1122.

Ringach, D. L. (2002). Spatial structure and symmetry of simple-cell receptive fields in macaque primary visual cortex. *Journal of Neurophysiology, 88*, 455–463.

Ringach, D. L., Shapley, R. M., & Hawken, M. J. (2002a). Orientation selectivity in macaque V1: Diversity and laminar dependence. *Journal of Neuroscience, 22*(13), 5639–5651.

Ringach, D. L., Bredfeldt, C. E., Hawken, M., & Shapley, R. (2002b). Suppression of neural responses to non-optimal stimuli correlates with tuning selectivity in macaque V1. *Journal of Neurophysiology, 87*, 1018–1027.

Robson, J. G. (1975). Receptive fields. In K. DeValois & R. DeValois (Eds.), *"Seeing" handbook of perception*. New York: Academic.

Rodieck, R. W. (1965). Quantitative analysis of cat retinal gangalion cell response to visual stimuli. *Vision Research, 5*, 583–601.

Sato, H., Katsuyama, N., Tamura, H., Hata, Y., & Tsumoto, T. (1996). Mechanisms underlying orientation selectivity of neurons in the primary visual cortex of the macaque. *Journal of Physiology, 494*, 757–771.

Shelley, M., McLaughlin, D., Shapley, R., & Wielaard, J. (2002). States of high conductance in a large-scale model of the visual cortex. *Journal of Computational Neuroscience, 13*, 93–109.

Sirovich, L. & Uglesich, R. (2004). The organization of orientation and spatial frequency in primary visual cortex. *Proceedings of the National Academy of Science of the United States of America, 101*, 16941–16946.

Tao, L., Cai, D., McLaughlin, D., Shelley, M., & Shapley, R. (2006). Orientation selectivity in visual cortex by fluctuation-controlled criticality. *Proceedings of the National Academy of Science of the United States of America, 103*, 12911–12916.

Tao, L., Shelley, M., McLaughlin, D., & Shapley, R. (2004). An egalitarian network model for the emergence of simple and complex cells in visual cortex. *Proceedings of the National Academy of Science of the United States of America, 101*(1), 366–371.

Troyer, T. W., Krukowski, A. E., Priebe, N. J., & Miller, K. D. (1998). Contrast-invariant orientation tuning in cat visual cortex: Thalamocortical input tuning and correlation-based intracortical connectivity. *Journal of Neuroscience, 18*, 5908–5927.

von der Heydt, R., Peterhans, E., & Dsteler, M. R. (1992). Periodic-pattern-selective cells in monkey visual cortex. *Journal of Neuroscience, 12*, 1416–1434.

Wielaard, D. J., Shelley, M., McLaughlin, D., & Shapley, R. (2001). How simple cells are made in a nonlinear network model of the visual cortex. *Journal of Neuroscience, 21*, 5203–5211.

Xing, D., Ringach, D., Shapley, R., & Hawken, M. (2004). Correlation of local and global orientation and spatial frequency tuning in macaque V1. *Journal of Physiology, 557*, 923–933.

Yoshimura, Y., & Callaway, E. M. (2005). Fine-scale specificity of cortical networks depends on inhibitory cell type and connectivity. *Nature Neuroscience, 8*, 1552–1559.